Chapter-5

Numerical Procedures and Geometry Analyzed

5.1 Introduction

The constitutive relations explained in the previous chapter will now be converted to rate tangent form (Pierce et al., 1984) and then to finite element equations before implementing into finite element code to analyze the crack tip deformation and fields in plastically compressible rate dependent solids. The advantages to use FEM over other numerical techniques are numerous. This is a versatile method in terms of structural geometry and material models. Complex shapes and structural components comprising different material properties also having material anisotropy are easily represented. The displacements or stress on the boundary nodes or elements of the idealized structure may be forced and the solutions of the unknowns at other locations within the body may be sought. Moreover, the method generates equilibrium equations producing usually a symmetric and positive definite matrix, which may be arranged in a banded form and solved with comparatively lesser storage and time. In the present chapter we will discuss the numerical procedure which is used to solve the problem and detailed description of geometry used for the present analysis.

5.2 Description of Analyses

The application of elastic-viscoplastic finite element technique in stress analysis due to various types of loads has become widespread and solutions of various complicated problems in fracture mechanics are now available. Such numerical techniques are inherently well suited for interpretation of the local effects in crack problems or similar situations where complex stress distributions are involved.

In the field of nonlinear fracture mechanics, a lot of work has been reported on various structural geometries subjected to mechanical loadings. Apart from the case of materials where classical plasticity theory is applicable for the analysis of deformation and fracture, some relatively new materials with their application areas as mentioned above exhibit plastic volume changes and/or pressure sensitive flow strength. When plastic compressibility is coupled with material softening, there is local intensification of crack tip opening accompanied by lower effective stress, which may affect crack propagation or eventual breakdown of a structure. Even though incorporating the effects of viscoplastic deformation ahead of a crack under different loading conditions require time-consuming and elaborate solutions steps but the availability of finite element technique provide means to deal with these difficult situations. Therefore, the computational model which includes unique characteristics like hardening-softening-hardening response, strain rate dependence, and plastically compressible solids with plastic non-normality, described in the previous chapter may be estimated by numerical assessment based on FEM technique. With these views in mind, using FORTRAN a finite element finite deformation code has been developed in this work for the simulation purpose and for plotting in Tecplot a preplot code also has been developed.

5.2.1 Problem Formulation

We briefly describe here the formulation of the quasi-static initial/ boundary value problem. In the present finite element analysis a convected coordinate Lagrangian formulation of the field equations is used with the independent variables being the particle positions in the initial stress free configuration and time. All field equations are taken to be functions of convected coordinates, y^{i}, which serve as particle labels, and time, t. Such kind of

formulation has extensively been employed previously, as in (Hutchens et. al., 2011; Needleman et. al., 2012; Mohan et. al., 2013; Khan et. al., 2017). For quasi-static deformations and in absence of body forces the principle of virtual work can be written as

$$\int_V \tau^{ij}\, \delta E_{ij} dV = \int_S T^i\, \delta u_i dS \qquad (5.1)$$

Where, τ^{ij} are the contravariant components of Kirchhoff stress in the deformed convected coordinate. V is volume and S is surface, of the body in the reference configuration. The nominal traction and Lagrangian strain components are, respectively given by

$$T^i = \left(\tau^{ij} + \tau^{kj} u^i_{,k}\right) v_j \qquad (5.2)$$

And

$$E_{ij} = \frac{1}{2}\left(u_{i,j} + u_{j,i} + u^k_{,i} u_{k,j}\right) \qquad (5.3)$$

Where, v_j and u_j are components of the reference surface normal and displacement vector on the reference base vectors, respectively, and $(\,)_{,i}$ denotes covariant differentiation in the reference frame.

For the solution of boundary value problems, incremental equilibrium equations are required owing to material path dependence. When the current values of all field quantities are assumed known, e. g. Kirchhoff stresses τ^{ij}, Lagrangian strains E_{ij}, displacements u_i and nominal tractions T^i, the conditions for satisfying incremental equilibrium during a time step Δt are obtained by expanding the Eq. (5.1) about the current state to obtain

$$\Delta t \int_{V} \left(\dot{\tau}^{ij} \delta E_{ij} + \tau^{ij} \dot{u}^{k}_{,i} \delta u_{k,j} \right) dV =$$

$$\Delta t \int_{S} \dot{T}^{i} \, \delta u_{i} dS - \left[\int_{V} \tau^{ij} \, \delta E_{ij} dV - \int_{S} T^{i} \, \delta u_{i} dS \right] \qquad (5.4)$$

Here, V and S are the volume and surface, respectively, of the body in the reference configuration, $\dot{(\,)} = \partial(\,)/\partial t$ at fixed y^{i}. The prescribed increment of the parameter t is Δt, so that the corresponding increments in stresses, strains, displacements and tractions are $\Delta\tau^{ij} = \dot{\tau}^{ij}\Delta t$, $\Delta E_{ij} = \dot{E}_{ij}\Delta t$, $\Delta u_{i} = \dot{u}_{i}\Delta t$ and $\Delta T^{i} = \dot{T}^{i}\Delta t$, respectively. The second term on the right hand side represents an equilibrium correction term. This equilibrium correction term is added to the incremental virtual work condition in order to avoid drifting off the solution from the true equilibrium path due to the finite time increments. The bracketed terms in equation (5.4) vanish if the current state satisfies equilibrium. However, in linear incremental analysis the solution tends to drift away from the true equilibrium path, and including the bracket terms in equation (5.4) tends to avoid such drifting.

5.2.2 Rate Tangent Formulation

Since numerical stability is always a key concern, we calculate the deformation history here, in a linear incremental manner and in order to increase the stable time step, the rate tangent modulus method proposed by Peirce et. al. (1984) is used. This rate tangent modulus method is one step time integration method for studying the quasi-static deformations of solids characterized by elastic-viscoplastic constitutive relations. This numerical procedure is aimed for use in combination with the displacement based finite element method. This approach is a forward gradient method and is based on an estimate of the viscoplastic strain rate in the interval between time t and $t + \Delta t$. The plastic strain rate in Eq. (4.5) is written as

$$\dot{\varepsilon}_{\mathrm{p}} = (1-\theta)\dot{\varepsilon}_{\mathrm{p(t)}} + \theta\dot{\varepsilon}_{\mathrm{p(t+\Delta t)}} \tag{5.5}$$

Where, the parameter θ can range from 0 to 1 ($\theta = 0$ corresponds to the explicit, Euler forward scheme). With the plastic strain rate being given as a function of the equivalent stress σ_{e}, its value at $t + \Delta t$ is estimated by using a Taylor series expansion. Expanding the above equation using Taylor series and up to first order gives

$$\dot{\varepsilon}_{\mathrm{p(t+\Delta t)}} = \dot{\varepsilon}_{\mathrm{p(t)}} + (\theta\Delta t)\left[\left.\frac{\partial\dot{\varepsilon}_{\mathrm{p}}}{\partial\sigma_{\mathrm{e}}}\right|_{\mathrm{t}}\dot{\sigma}_{\mathrm{e}} + \left.\frac{\partial\dot{\varepsilon}_{\mathrm{p}}}{\partial\varepsilon_{\mathrm{p}}}\right|_{\mathrm{t}}\dot{\varepsilon}_{\mathrm{p}}\right] \tag{5.6}$$

Initially let's formulate the rate tangent expression for the case when the constitutive equation is said to follow normality flow rule. After combining equations (4.1), (4.2) and (4.3) and solving for $\hat{\tau}^{ij}$ gives

$$\hat{\tau}^{ij} = L^{ijkl}\dot{E}_{kl} - \dot{P}^{ij} \tag{5.7}$$

Where, $\dot{P}^{ij} = \left(\frac{3\dot{\varepsilon}_{\mathrm{p}}}{2\sigma_{\mathrm{e}}}\right)L^{ijkl}p_{\mathrm{kl}}$ (5.8)

Using equations (4.2) and (4.7)

$$\dot{\sigma}_{\mathrm{e}} = \frac{3}{2\sigma_{\mathrm{e}}}\hat{\tau}^{ij}p_{\mathrm{ij}} = \frac{3}{2\sigma_{\mathrm{e}}}p_{\mathrm{ij}}L^{ijkl}D_{\mathrm{kl}} - \frac{3}{2\sigma_{\mathrm{e}}}p_{\mathrm{ij}}L^{ijkl}D^{\mathrm{p}}_{\mathrm{kl}} \tag{5.9}$$

After defining the terms

$$H = \left[\left(\frac{3}{2\sigma_{\mathrm{e}}}\right)p_{\mathrm{ij}}P^{ij} - \frac{\partial\dot{\varepsilon}_{\mathrm{p}}/\partial\varepsilon_{\mathrm{p}}}{\partial\dot{\varepsilon}_{\mathrm{p}}/\partial\sigma_{\mathrm{e}}}\right] \tag{5.10}$$

$$P^{ij} = \left(\frac{3}{2\sigma_{\mathrm{e}}}\right)L^{ijkl}p_{\mathrm{kl}} \tag{5.11}$$

$$\xi = (\theta\Delta t)\frac{\partial\dot{\varepsilon}_{\mathrm{p}}}{\partial\sigma_{\mathrm{e}}}H \tag{5.12}$$

the expression for $\dot{\varepsilon}_p$ can be written as

$$\dot{\varepsilon}_{\mathrm{p}} = \frac{\dot{\varepsilon}_{\mathrm{p(t)}}}{1+\xi} + \frac{\xi}{H+H\xi} P^{ij} D_{\mathrm{ij}} \tag{5.13}$$

After putting the value of $\dot{\varepsilon}_{\mathrm{p}}$ from equation (5.13) in equation (5.7), the rate tangent expression for the Jaumann derivative of Kirchhoff stress finally leads to

$$\hat{\tau}^{ij} = \left(L^{ijkl} - \frac{\xi}{H+H\xi} P^{ij} P^{kl}\right) D_{\mathrm{kl}} - \frac{\dot{\varepsilon}_{\mathrm{p(t)}}}{1+\xi} P^{ij} \tag{5.14}$$

Similarly, when the constitutive equation is said to follow non-normality flow rule, the rate tangent expression for the Jaumann derivative of Kirchhoff stress can be derived as follows:

$$\dot{\sigma}_{\mathrm{e}} = \frac{3}{2\sigma_{\mathrm{e}}} \hat{\tau}^{ij} q_{\mathrm{ij}} = \frac{3}{2\sigma_{\mathrm{e}}} q_{\mathrm{ij}} L^{ijkl} D_{\mathrm{kl}} - \frac{3}{2\sigma_{\mathrm{e}}} q_{\mathrm{ij}} L^{ijkl} D^{\mathrm{p}}_{\mathrm{kl}} \tag{5.15}$$

After defining the terms

$$H = \left[\left(\frac{3}{2\sigma_{\mathrm{e}}}\right) p_{\mathrm{ij}} Q^{ij} - \frac{\partial \dot{\varepsilon}_{\mathrm{p}} / \partial \varepsilon_{\mathrm{p}}}{\partial \dot{\varepsilon}_{\mathrm{p}} / \partial \sigma_{\mathrm{e}}}\right] \tag{5.16}$$

$$Q^{ij} = \left(\frac{3}{2\sigma_{\mathrm{e}}}\right) L^{ijkl} q_{\mathrm{kl}} \tag{5.17}$$

$$\xi = (\theta \Delta t) \frac{\partial \dot{\varepsilon}_{\mathrm{p}}}{\partial \sigma_{\mathrm{e}}} H \tag{5.18}$$

the expression for $\dot{\varepsilon}_{\mathrm{p}}$ can now be written as

$$\dot{\varepsilon}_{\mathrm{p}} = \frac{\dot{\varepsilon}_{\mathrm{p(t)}}}{1+\xi} + \frac{\xi}{H+H\xi} Q^{ij} D_{\mathrm{ij}} \tag{5.19}$$

After putting the value of $\dot{\varepsilon}_{\mathrm{p}}$ from equation (5.19) in equation (5.7), the rate tangent expression for the Jaumann derivative of Kirchhoff stress finally leads to

$$\hat{\tau}^{ij} = \left(L^{ijkl} - \frac{\xi}{H+H\xi} Q^{ij} P^{kl}\right) D_{\mathrm{kl}} - \frac{\dot{\varepsilon}_{\mathrm{p(t)}}}{1+\xi} P^{ij} \qquad (5.20)$$

5.2.3 Finite Element Equations

Here the full derivation of the finite element equations has been provided as an approximate solution of a variational principle in terms of a displacement field with a finite number of degrees of freedom. When viscous effects are accounted for, the problem is time - dependent, and here we let a parameter t in equation (5.4) denotes time so that ($\dot{}$) denotes the time derivative.

For elastic-viscoplastic problems the constitutive relations are typically of the form (as observed from equations 5.14 and 5.20)

$$\hat{\tau}^{\mathrm{ij}} = L_*^{\mathrm{ijkl}} \dot{E}_{kl} + \hat{\tau}_*^{\mathrm{ij}} \qquad (5.21)$$

In some cases the stress rate term $\hat{\tau}_*^{\mathrm{ij}}$ includes all viscous effects. In other cases, where forward gradient methods have been used to increase the maximum stable step size Δt in the numerical solution, $\hat{\tau}_*^{\mathrm{ij}}$ may represent only part of the viscous effects.

In the finite element method the volume V in the reference state is divided into K subvolumes (i. e. K elements), such that

$$\mathrm{V} = \sum_{\mathrm{k=1}}^{\mathrm{K}} \mathrm{V}_{\mathrm{(K)}} \,, \mathrm{S} = \sum_{\mathrm{k=1}}^{\mathrm{K}} \mathrm{S}_{\mathrm{(K)}} \qquad (5.22)$$

Inside the volume $\mathrm{V}_{\mathrm{(K)}}$ the displacement components $\mathrm{u_i}$ are expressed in terms of $\mathrm{F_e}$ different displacement fields $\mathrm{U_i^{(n)}}$, such that

$$\dot{\mathrm{u}}_{\mathrm{i}} = \sum_{\mathrm{n=1}}^{\mathrm{F_e}} \mathrm{U_i^{(n)}} \dot{\mathrm{D}}_{\mathrm{(n)}} \,, \dot{\mathrm{E}}_{\mathrm{ij}} = \sum_{\mathrm{n=1}}^{\mathrm{F_e}} \mathrm{E_{ij}^{(n)}} \dot{\mathrm{D}}_{\mathrm{(n)}} \,,$$

$$E_{ij}^{(n)} = \frac{1}{2}\left(U_{i,j}^{(n)} + U_{j,i}^{(n)} + u_{,i}^{k}U_{k,j}^{(n)} + u_{,j}^{k}U_{k,i}^{(n)}\right) \qquad (5.23)$$

Here, F_e denotes the number of degree of freedom for the element, $U_i^{(n)}\left(\xi_j\right)$ are the corresponding shape functions, and $D_{(n)}$ are the node point displacements. Node points are mostly located at element boundaries, and neighbouring elements use the same node points at the common element interface. The shape functions are assumed to be specified such that the displacements are continuous across element boundaries, when the common node points have the same displacement values. In the present analysis quadrilateral elements comprised of four crossed linear displacement triangular elements have been used for discretization, Fig. 5.1. For the planer, 3 noded element used in fig 5.2 each node has 2 degree of freedom, so that the number of degrees of freedom for the element is 6.

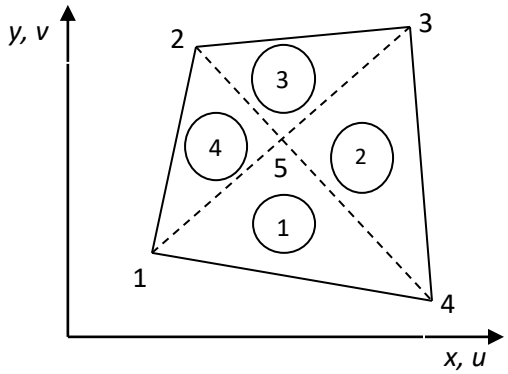

Figure 5.1: The condensation of internal node in quadrilateral element comprised of four crossed constant strain triangular elements

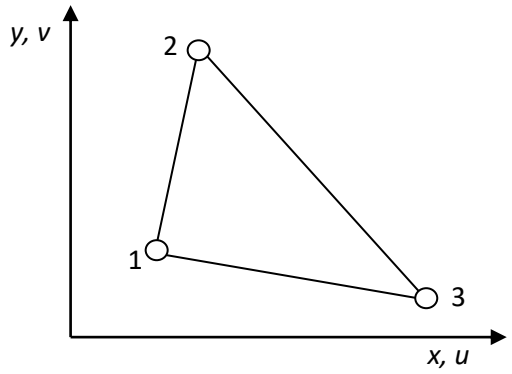

Figure 5.2: Triangular finite element

If the internal virtual work is denoted by δW_{int} and the external virtual work is denoted by δW_{out}, the incremental principle of virtual work (5.4) can be written as

$$\Delta(\delta W_{int.}) = \Delta(\delta W_{ext.}) + \Delta(\delta W_{corr.}) \qquad (5.24)$$

Where $\Delta(\delta W_{corr.})$ is the equilibrium correction term. Using (5.22) in (5.4), each of terms in equation (5.24) comes out as a sum over the elements

$$\sum_{k=1}^{K} \Delta(\delta W_{int.})_{(k)} = \sum_{k=1}^{K} \Delta(\delta W_{ext.})_{(k)} + \sum_{k=1}^{K} \Delta(\delta W_{corr.})_{(k)} \qquad (5.25)$$

Now, the virtual displacements,δu_i, for which equation (5.4) is satisfied, can be chosen as the finite element approximation of the displacement field corresponding to one nodal displacement, $D_{(M)} = 1$, with all other nodal displacement equal to zero. Thus, with δu_i replaced by $U_i^{(m)}$, and with equation (5.23) substituted into (5.25), the contributions from each element take the form

$$\Delta(\delta W_{int.})_{(k)} = \sum_{n=1}^{F_e} A_{(mn)} \Delta D_{(n)} \qquad (5.26)$$

$$\Delta(\delta W_{ext.})_{(k)} = \Delta B_{(m)} \qquad (5.27)$$

$$\Delta(\delta W_{corr.})_{(k)} = \Delta C_{(m)} \qquad (5.28)$$

Here, $\Delta D_{(n)} = \Delta t D_{(n)}$, and the element stiffness matrix $A_{(mn)}$, the load increment vector $\Delta B_{(m)}$, and the equilibrium correction vector $\Delta C_{(m)}$ are given by

$$A_{(mn)} = \int_{V(k)} \left(L_*^{ijkl} E_{kl}^{(n)} E_{ij}^{(m)} + \tau^{ij} g^{kl} U_{l,i}^{(n)} U_{k,j}^{(m)} \right) dV \qquad (5.29)$$

$$\Delta B_{(m)} = \Delta t \int_{V(k)} -\hat{\tau}_*^{ij} E_{ij}^{(m)} dV + \Delta t \int_{S(k)} \dot{T}^i U_i^{(m)} dS \qquad (5.30)$$

$$\Delta C_{(m)} = \left[- \int_{V(k)} \tau^{ij} E_{ij}^{(m)} dV + \int_{S(k)} T^i U_i^{(m)} dS \right] \qquad (5.31)$$

Finite element solutions make use of a connectivity matrix, which specifies the global node number corresponding to a local node number in a given element. From these connectivities one easily obtains the global degree of freedom no. N corresponding to the local degree of freedom no. n in element no. k, i.e. N = N (n, k). These relations are needed to replace all local numbers by global numbers when the summations in equation (5.25) are carried out to obtain the system of liner algebraic equations

$$\sum_{N=1}^{F} A_{(MN)} \Delta D_{(N)} = \Delta B_{(M)} + \Delta C_{(M)} \qquad (5.32)$$

For $M = 1,2, \ldots . F$

Here, F is the global number of degrees of freedom in the finite element model, $A_{(MN)}$is the global stiffness matrix, etc.

After solving equation (5.32), the nodal displacement increments $\Delta D_{(N)}$ are used in equation (5.23), element by element, to calculate the strain increments ΔE_{ij} in the integration points, from which stress increments $\Delta\tau^{ij}$ in the integration points are obtained using equation (5.21). The current values of the stresses after the increments are updated by calculating $\tau^{ij} + \Delta\tau^{ij}$ for each integration point, and the current values of the nodal displacement are updated by calculating $D_{(M)} + \Delta D_{(M)}$.

5.2.4 Geometry Description

Due to the widespread use of plate structures of complex geometry in practical problems, their analyses have become very important in engineering practice. Cracks in plates of finite size and shapes are of great practical interest even though for these cases no closed form solutions of fracture parameter are available. Further, FEM achieved remarkable success in static and dynamic analyses of cracked plate problems in fracture parameter estimation. Here, plain strain calculations are carried out for a semi circular region of radius R_0=2.0 in arbitrary units as shown in Fig.5.3a. The loading and the geometry are symmetric with respect to the crack plane. There is a notch of initial radius b_0 =0.001 in the same arbitrary units with its centre at the origin of the coordinate system as shown in figure 5.3b, so that $R_0/b_0 = 2\,x\,10^3$. The aim is to simulate small scale yielding conditions for which plastic zone sizes remain small compared to R_0. Although different crack tip shapes are possible from the point of view of plastic slip geometry (McClintok, 1971), the semicircular one seems to be a suitable averaging.

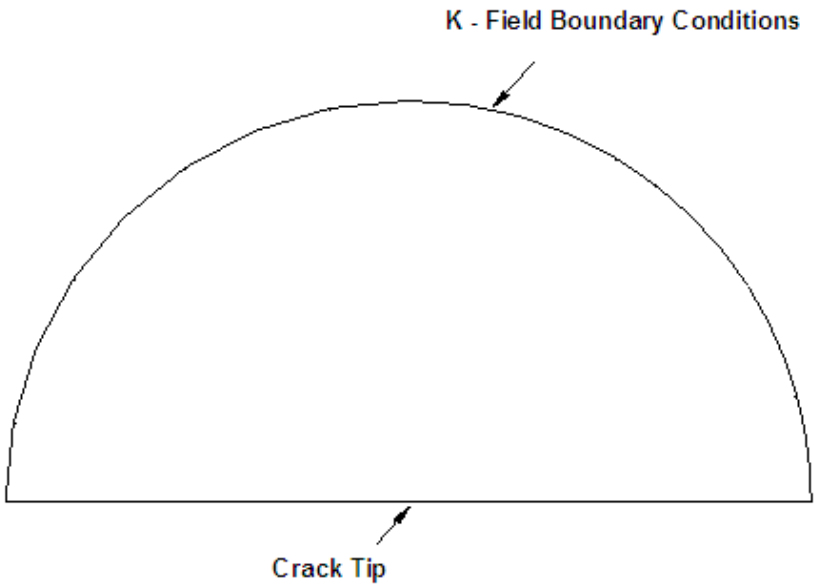

(a)

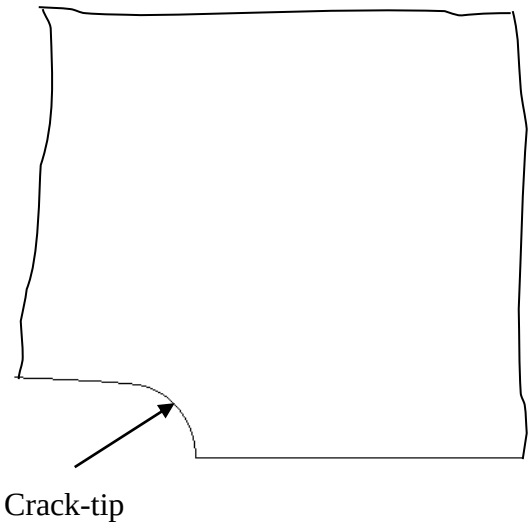

(b)

Figure 5.3: Geometry used in the finite element simulation of small scale yielding with K-field boundary conditions; a) Full geometry and b) portion of the geometry showing the crack tip

5.3 Finite Element Issues

This section presents some of the basic finite element issues related to the present computational model used in the estimation of the crack tip fields and crack tip deformation. The purpose of this brief description is to familiarize the readers, who are not very conversant with the basic features of FEM techniques.

5.3.1 Element Description

There are various types of element geometries, which are commonly used in finite element analyses. The interpolation functions used depend not only on the number of nodes in the element but also on the element shape. The shape of the element should be such that its geometry is uniquely defined by a set of points, which are the element nodes, used in the description of interpolation functions. In the present analysis quadrilateral elements, each comprised of four "crossed" constant strain triangular elements have been used for mesh generation. This crossed-triangle configuration also helps to avoid volumetric locking. Such type of elements, with a proper aspect ratio and orientation, are widely used to reproduce localized deformation pattern in case of finite strains.

As quadrilateral elements with four crossed triangular element is used then due to these four crossed such elements one extra node will be there to connect all four crossed elements as shown in figure 5.4. So the total number of nodes will be 5 in place of four nodes. If all elements are with 2 degree of freedom per node then total number of degrees of freedom will be 10. Thus the size of the assembled stiffness matrix is 10 x 10. When merging the element into a mesh, in order to reduce the number of algebraic equations, the internal degree of freedom of 5^{th} node should be eliminated or condensed. The technique for deleting the

unwanted degree of freedom is known as condensation. As the dynamic effects are ignored in the condensation process, this method is usually called static condensation. Consequently, only the degrees of freedom associated with the external nodes enter the equations and the stiffness matrix dimension becomes 8 x 8. The stiffness matrices of the four triangular elements should be superimposed in order to create the stiffness matrix of the quadrilateral element. The static condensation processed has been described in Appendix.

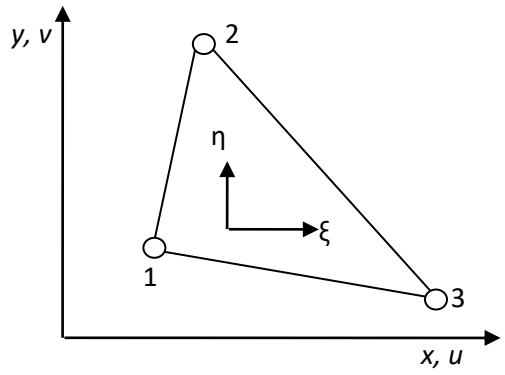

Figure 5.4: Triangular finite element and it's representation in the local coordinate system

A 3-noded constant strain triangular element is described here in some detail. This is a planar element with $u^3 \equiv 0$. Thus each node has 2 degrees of freedom, corresponding to the nodal displacements in the x^1 and x^2 directions, respectively. The element is used for conditions of plane strain problems. The local node numbers are specified in the Fig. 5.4 and (ξ_r, η_r) denotes the values of the coordinates in node number r. Then shape functions $U_i^{(n)}$ can be expressed in terms of 3 functions $\phi_r(\xi, \eta)$, specified by

$\phi_r(\xi, \eta) = \xi$ for $r = 1$

$= \eta$ for $r = 2$

$= 1 - \xi - \eta$ for $r = 3$ (5.33)

It is emphasized that here r is not a tensor index, but is used to denote the local node number. Now the same functions $\phi_{\mathrm{r}}(\xi, \eta)$are used to express the Cartesian coordinates (x, y) of a point (ξ, η)inside the element

$$\mathrm{x} = \sum_{\mathrm{r}=1}^{3} \phi_{\mathrm{r}}(\xi, \eta) x_{\mathrm{r}}, \ \mathrm{y} = \sum_{\mathrm{r}=1}^{3} \phi_{\mathrm{r}}(\xi, \eta) y_{\mathrm{r}} \quad (5.34)$$

such that the mapping is completely specified by giving the coordinate values $(x_{\mathrm{r}}, y_{\mathrm{r}})$ of the 3 nodal points. With $(u_{\mathrm{r}}, v_{\mathrm{r}})$ denoting the displacements of nodal point no. r in the x and y directions, the displacement fields are approximated by

$$\mathrm{u} = \sum_{\mathrm{r}=1}^{3} \phi_{r}(\xi, \eta) u_{\mathrm{r}}, \ \mathrm{v} = \sum_{\mathrm{r}=1}^{3} \phi_{r}(\xi, \eta) v_{\mathrm{r}} \quad (5.35)$$

By comparing with the notation in expression (5.23), it is seen that the nodal displacements are

$$\left(D_{(2\mathrm{r}-1)}, D_{(2\mathrm{r})}\right) = (u_{\mathrm{r}}, v_{\mathrm{r}}) \quad (5.36)$$

and the shape functions are

$$\left(\mathrm{U}_1^{(2\mathrm{r}-1)}, \mathrm{U}_2^{(2\mathrm{r}-1)}\right) = (\phi_{\mathrm{r}}(\xi, \eta), 0) \quad (5.37)$$

$$\left(\mathrm{U}_1^{(2\mathrm{r})}, \mathrm{U}_2^{(2\mathrm{r})}\right) = \left(0, \phi_{\mathrm{r}}(\xi, \eta)\right) \quad (5.38)$$

for $\mathrm{r} = 1,2,3$

Now the shape functions U_i^n are given as functions of ξ and η: but in order to find the expressions for $E_{ij}^{(n)}$ in (5.23) we need to find the covariant derivatives and thus also the partial derivatives with respect to x and y. The chain rule gives

$$\begin{Bmatrix} \frac{\partial \phi_r}{\partial \xi} \\ \frac{\partial \phi_r}{\partial \eta} \end{Bmatrix} = \begin{bmatrix} \frac{\partial x}{\partial \xi} & \frac{\partial y}{\partial \xi} \\ \frac{\partial x}{\partial \eta} & \frac{\partial y}{\partial \eta} \end{bmatrix} \begin{Bmatrix} \frac{\partial \phi_r}{\partial x} \\ \frac{\partial \phi_r}{\partial y} \end{Bmatrix} = J \begin{Bmatrix} \frac{\partial \phi_r}{\partial x} \\ \frac{\partial \phi_r}{\partial y} \end{Bmatrix} \tag{5.39}$$

Where J is the Jacobi matrix for the coordinate transformation. Inverting the relationship gives

$$\begin{Bmatrix} \frac{\partial \phi_r}{\partial x} \\ \frac{\partial \phi_r}{\partial y} \end{Bmatrix} = J^{-1} \begin{Bmatrix} \frac{\partial \phi_r}{\partial \xi} \\ \frac{\partial \phi_r}{\partial \eta} \end{Bmatrix} \tag{5.40}$$

Which gives the partial derivatives of the shape functions with respect to x and y as needed.

5.3.2 Mesh Generation

The mesh generation for the two-dimensional geometry was performed using the GRIDGN subroutine of the code without the use of any special crack tip elements. Adequate mesh refinement is always an issue when carrying out finite element solutions with an objective to capture accurate stress and strain gradients of interest in fracture mechanics but excessive refinement are generally avoided to reduce unnecessary long run time. In the present analyses adequate mesh size was obtained based on the mesh convergence studies described in next chapter.

5.3.3 Material Model

Figure 5.5 shows the hardness function $g(\varepsilon_p)$ of four different materials B, C, E and G as mentioned in (Mohan et. al., 2013). In order to compare the effect of hardening-softening-hardening type hardness function in contrast to the bilinear hardening-hardening type, we consider materials B and C. In materials B and C, h_2 is positive and $h_2 = h_3$; so the value of ε_2 is irrelevant here. When $h_1 > 0$, $h_2 < 0$ and $h_3 > 0$, the parameters h_1, h_2 and h_3 give a hardening-softening-hardening relation. The value of ε_1 specifies the plastic strain at which the hardening slope is changed for material B and C whereas material E and G at this strain, transition from hardening to softening takes place and ε_2 species the strain at which the transition back to hardening occurs. The parameters $h_1$and ε_1 are fixed at $h_1 = 24$ and $\varepsilon_1 = 0.085$ for all four materials while the value of $h_2 = 5.0$ for material B and for material C it is 1.0. For material E, $h_2 = -3.90$, $h_3 = 15.0$, $\varepsilon_2 = 0.6$ and for material G, $h_2 = -3.90$, $h_3 = 15.0$, $\varepsilon_2 = 5.0$.

The constant parameters considered for the present analysis are E/σ_0=100, reference strain rate $\dot{\varepsilon}_1 = 1\ s^{-1}$ and rate hardening exponent m = 0.02. While these parameters in the present model have been considered constant, for actual materials their values may depend on strain rate and temperature.

The parameters varied in Eq. (4.6) are h_2, h_3 and ε_2. For material G with $h_2 = -3.90$, $g(\varepsilon_p)$ would vanish at about $\varepsilon_p = 0.77$. To preclude this in the calculations, the minimum value of $g(\varepsilon_p)$ is set to $0.1\sigma_0$ so that for this material, $g(\varepsilon_p) = 0.1\sigma_0$ for $0.77 \leq \varepsilon_p \leq 5$.

Results are presented for two values of α_p, $\alpha_p = 0.333333$ and $\alpha_p = 0.28$. The value of α_p is related to the plastic Poisson's ratio via Needleman at al. (2015)

$$\nu_p = \frac{\alpha_p}{1-\alpha_p} \tag{5.41}$$

so that $\alpha_p = 1/3$ corresponds to $\nu_p = 1/2$ (a plastically incompressible solid); $\alpha_p = 0.28$ corresponds to $\nu_p = 0.389$ and α_{DF} =0.849. The results obtained with $\alpha_p = 0.333333$ ($\nu_p = 0.499997$, $\alpha_{DF} \approx 0$) will be referred to subsequently as corresponding to a plastically incompressible solid. It is worth noting that because of the assumed plastic compressibility $(\alpha_p \neq 1/3)$ implies hydrostatic stress dependent plastic flow.

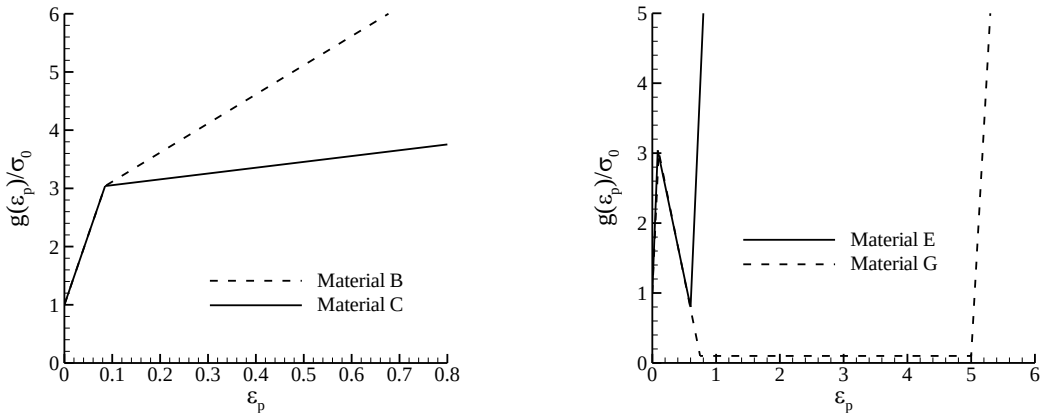

(a) (b)

Figure 5.5: The variation of hardness function $g(\varepsilon_p)$ with plastic strain ε_p.a) material B ($h_2 = h_3 = 5.0$) and material C ($h_2 = h_3 = 1.0$), b) material E ($h_2 = -3.90$, $h_3 = 15.0$) and material G $\left(h_2 = -3.90, h_3 = 15.0, \varepsilon_2 = 5.0\right)$ (Mohan et. al., 2013)

5.3.4 Equation Solver and Solution Control Options

The equation solver used by the present work is based on the size of the problem and in this investigation the Cholesky decomposition solver was used. Cholesky decomposition is a special version of LU decomposition and this can handle symmetric matrices more efficiently. For a symmetric matrix A, by definition, we know that $a_{ij} = a_{ji}$. LU decomposition is not efficient enough for handling symmetric matrices. The computational load can be halved when we use Cholesky decomposition. This procedure approximates a solution to within a specified convergence tolerance. The details of the Cholesky decomposition method are provided in Appendix.

Here integration is performed using present rate tangent formulations of the constitutive equations. Fixed time steps have been used rather than the adaptive time stepping. The deformation history is calculated using a linear incremental update with time step size $dt = 0.0002$ s. This breaks each of the load steps into smaller steps to ease convergence.

5.4 Concluding Remarks

In this chapter, initially the problem formulation has been presented while using the rate form of the virtual work principle. A rate tangent method has been used for the constitutive update. As the rate tangent formulation of the constitutive equations is in the classical form of elastic-viscoplastic equations, these constitutive equations have further been converted into finite element equations. The geometry on which the plane strain calculations are carried out has been described next. Some finite element issues in the context of the present problems are also briefly described and finally, some typical aspects of computational procedure in the

context of finite element technique have been described. The next chapter contains the descriptions of various results obtained from the numerical studies.